Chapter 2

Production and Characterization of Fast Mixed He Beams

As mentioned in the previous chapter the expectation that HeI beam emission could be used as electron temperature diagnostics is, among other reasons, based on the different energy dependence of the excitation of spin conserving and spin changing collisions. It was therefore felt useful to examine how the composition of a fast neutral He beam could be influenced with respect to its metastable fraction. Hence, fast He-atom beams with a comparably high metastable fraction (so-called mixed beams) were produced and analyzed in this part of the work. The actual experiments on tokamak plasmas have finally been performed by using the existing heating beam facilities, and modelling calculations revealed that the metastable population in the beam will be produced and destroyed more or less independently of the initial population. Furthermore it was discovered from calculations in view of the sensitivity of emission lines with respect to T_e and n_e (chapter 4.2) that a low metastable fraction in the beam is generally advantageous. Nevertheless, a brief description of the experimental setup at Institut für Allgemeine Physik (IAP), TU Wien, and the underlying physics will be given in the following chapters. The results of the experiments are discussed in chapter 2.3.

2.1 Underlying Physics

The following subsections deal with the physics for the production and characterization of mixed He beams.

2.1.1 Production of Mixed He Beams

Neutral He beams are produced from accelerated ion beams by charge-exchange collisions in a so-called neutralization cell. After neutralization, the remaining ions are removed from of the beam. A description of the applied ion source (2.45 GHz ECRIS [44, 45, 46]), the beam transport system, and the neutralization chamber [47] is given in chapter 2.2.

The probability for charge-exchange processes in the neutralization cell is strongly dependent on the energy defect ΔE between binding energies of the active electron after ($E_{B,beam}$) and before the collision ($E_{B,target}$):

$$\Delta E = E_{B,beam} - E_{B,target} \,. \tag{2.1}$$

For the energy range used (1 - 3 keV/amu) the charge-exchange process is resonant for processes with $\Delta E = 0$ or quasiresonant for $\Delta E \approx 0$ as the electron velocity is large compared to the velocity of the projectile ion.

In order to produce a He-atom beam with a high ground-state fraction, He gas is used as target, since the charge-exchange process is resonant:

$$He^+ + He^0\ (1^1S) \rightarrow He^0(1^1S) + He^+.$$

state	E_B
$He(1^1S)$	24.6 eV
$He(2^3S)$	4.77 eV
$He(2^1S)$	3.97 eV
$He(2^3P)$	3.63 eV
$He(2^1P)$	3.37 eV

Table 2.1: Binding energy E_B of He states with principal quantum numbers $n \leq 2$ [48].

The binding energy of the five lowest HeI levels are given in table 2.1. For the production of He-atom beams with high metastable fractions, targets with ionization energies close to the binding energies of the metastable levels $He(2^1S)$ and $He(2^3S)$ are advantageous. This is the case for alkalines. The binding energies of the valence electrons of ground-state Cs, Li, K, and Na and the corresponding energy defects for charge exchange into metastable

element	E_B	$\Delta E(2^1\mathrm{S})$	$\Delta E(2^3\mathrm{S})$
Cs	3.89 eV	**0.08**	0.88
K	4.34 eV	**-0.37**	0.43
Na	5.14 eV	-1.17	**-0.37**
Li	5.39 eV	-1.42	-0.62

Table 2.2: Binding energy E_B of the valence electrons of ground-state Cs, Li, K, and Na [50] and the corresponding energy defects for charge exchange into He(2^1S) and He(2^3S), respectively.

He(2^1S) and He(2^3S), respectively, are given in table 2.2. These charge-exchange reactions are quasiresonant and take place with large cross sections [49].

The highest He(2^3S) fraction from neutralization of a He-ion beam in alkali vapour can be obtained by using Na vapour since Na shows a quite low energy defect with respect to He(2^3S) and a relatively large energy defect with respect to He(2^1S). For a rough estimate of the final population fractions of ground-state He and the two metastable states we consider the statistical weights of those He levels with binding energies comparable to those of Na, i.e. levels with principal quantum number $n = 2$. The possible values for the total angular momentum quantum number J of a particle determined by its spin quantum number S and orbital momentum quantum number L are given by:

$$J = L + S, L + S - 1, \ldots, |L - S|. \tag{2.2}$$

The statistical weight of a state specified by J is thus given by

$$\sum (2\,J + 1). \tag{2.3}$$

Table 2.3 shows S, L, J, and statistical weight for all He($n = 2$) states. If we neglect the probability of populating both ground state ($E_B = 24.6$ eV) and higher excited levels ($E_B \leq 1.86$ eV) due to their large energy defects with respect to ground-state Na, and if we additionally consider the four $n = 2$ levels as giving rise approximately to the same energy defect, we find population fractions F as shown in the last column of table 2.3.

level	S	L	J	$\sum(2J+1)$	F
He(2^3S)	1	0	1	3	18.75%
He(2^1S)	0	0	0	1	6.25%
He(2^3P)	1	1	0,1,2	9	56.25%
He(2^1P)	0	1	1	3	18.75%

Table 2.3: Spin- (S), orbital momentum- (L), total angular momentum quantum number (J), statistical weight $\sum(2J+1)$ for He states with principal quantum number $n = 2$ and the resulting population fractions F, see text.

The decay time of the 2^1P state into the ground state is approximately 0.6 ns with a branching ratio of 99.9% and 0.1 μs into the metastable 2^1S state for the remaining 0.1%. This results in a final population structure after relaxation of the excited levels:

$$75\%\ 2^3\text{S},\ 6.25\%\ 2^1\text{S},\ \text{and}\ 18.75\%\ 1^1\text{S}.$$

Since the energy defect for charge exchange from Na into He(2^3S) is much smaller than into any other level, the population fraction of the 2^3S level is even higher than estimated [51, 52].

The above consideration is only valid for thin targets without further collisions after the charge-changing process. In a thick target the neutralized particle will encounter further collisions and the population of metastable- and ground state can be rearranged. As spin-changing collisions have much smaller cross sections than spin-conserving collisions [53], an atom exited from He(2^3S) is likely to stay in the triplet system and decay back into He(2^3S) leaving the population of He(2^3S) unchanged. A particle excited from the He(2^1S) will predominantly decay into the ground state. For He(3^1P) the branching ratio is for example 97.6% into He(1^1S) and 2.4% into He(2^1S). Hence, in a thick target the metastable singlet state is likely to be quenched into the ground state by excitation processes.

Another attenuation mechanism for the metastable states is ionization. Respective cross sections are in general larger than excitation cross sections for collisions between fast metastable He atoms and gas atoms [54]. Ionization processes lead to a higher ground-state fraction in the beam since ionization cross sections for He(2^3S) and He(2^1S) are much larger than for ground state He [54]. In addition, high ionization cross sections for metastable He atoms also demand low residual gas pressure.

2.1.2 Beam Characterization

In the next chapter a survey of different techniques for measuring the metastable fraction in atomic and ionic beams is given. Chapter 2.1.2.2 describes the technique used at IAP.

2.1.2.1 Methods for Determination of Metastable Beam Fractions

Several techniques have been developed to measure the metastable fraction in atomic and ionic beams, e.g.:

- time-of-flight method,
- laser atom-absorption spectroscopy,
- laser-induced fluorescence,
- beam attenuation method,
- optical attenuation method, and
- grazing incidence method.

Time-of-flight method

Energy conservation requires that in a charge-changing collision the difference in binding energy of the electron before and after the collision will affect the kinetic energy of the collision partners. He atoms in the metastable state after the collision will therefore have a different kinetic energy than those in the ground state. Particles of a sufficiently short beam pulse will therefore separate while passing from the neutralization cell to the detector where they are registered. E.g., Reynaud *et al.* [51] determined the metastable fractions of 1^1S, 2^1S, and 2^3S in He beams ($E \leq 1.5$ keV) after neutralization of He-ion beams in Na, K, Cs, and Rb vapor. Prerequisites for this technique are beams with small energy spread and particle detection systems with high energy resolution.

Laser atom-absorption spectroscopy

A laser beam is attenuated when passing through the particle beam. As the absorption is related to the beam particle density, absorption measurements yield the line-integrated population density of the metastable atoms [55]:

$$\int n(x)dx = \frac{4\,\epsilon_o\, m_e\, c}{F\, e^2} \int ln\left(\frac{S_A(\lambda)}{S_0(\lambda)}\right) d\lambda\,, \tag{2.4}$$

where $n(x)$ stands for the metastable-population density at the position x and F for the oscillator strength. $S_A(\lambda)$ and $S_0(\lambda)$ denote the wavelength (λ) dependent transmitted intensity with and without sample, respectively. Christmann *et al.* [55] analysed energetic He beams produced by neutralization of He ions in Li vapor using the $2^3S \rightarrow 2^3P$ transition at 1083 nm to measure the He(2^3S) fraction.

Laser-induced fluorescence

Here, the beam is irradiated by laser light and the resulting fluorescence of the beam particles is registered. The wavelength of the laser light has to correspond to an allowed transition with the lower level being the level of interest. With this technique measurements of the 2^3S fraction in fast He beams have been performed by Dinklage [56]. The allowed transition $2^3S \rightarrow 3^3P$ was pumped. Observation of the resulting fluorescence light at 398 nm yielded the 2^3S density in the He beam.

Beam attenuation method

This technique, introduced by Gilbody *et al.* [57], is based on the substantial difference in the binding energies and, hence, ionization cross sections between ground- and metastable states. The particle beam passes through a well defined target (density n, interaction length L) and all beam atoms which are ionized are removed from the beam by an electrostatic field. With increasing target thickness $\Pi = n \cdot L$ the metastable population will be more and more reduced leaving only ground-state particles for a sufficiently thick target. The beam-particle intensity $I(\Pi)$ is measured from low target thicknesses (thin target) to large target thicknesses where the metastable atoms have been completely attenuated (thick target). Plotting $\ln I(\Pi)/\ln I(0)$ against target thickness gives a decaying curve. In the first section representing the thin target the intensity shows a linear decay which is dominated by the attenuation of the metastable levels which defines the slope of the curve. For increasing target density the metastable fraction becomes too small to contribute to the intensity. Consequently, the slope of the curve changes and becomes linear again for thick targets, where the attenuation of the ground state atoms defines the slope of the curve. From the slopes and the intercepts of these linear segments the ionization cross sections of the ground state, σ_{01}, and of the metastable states, σ_{m1} (both 2^1S and 2^3S), and the metastable fraction f can be derived.

The drawback of this method is that it does not discriminate between He(2^1S) and He(2^3S) due to the small difference of their binding energies. Furthermore, secondary processes influence the measured metastable fraction. Collisions with the target atoms not only result

in ionization but also de-excitation of the beam particles. Since these atoms are not removed from the beam by the electrostatic field, the measured fraction f_m of metastables is lower than the true fraction f [49]:

$$f_m = f \frac{\sigma_{m1} - \sigma_{01}}{\sigma_{m1} + \sigma_{m0} - \sigma_{01}} \tag{2.5}$$

where σ_{m0} stands for the de-excitation cross section of metastable atoms into the ground-state. This cross section has to be known since it can not be determined with this method.

Optical attenuation method (OAM)

This technique introduced by Matsumoto *et al.* [58] is based on the spectroscopic studies of Hollstein *et al.* [59] on de-excitation of He atoms involving metastable He(2^1S) and He(2^3S) atoms. In these measurements ion beams are attenuated by electron capture in suitable atomic targets. From the intensity of light emitted by the excited projectiles in the neutralization cell the electron-capture cross sections of the initial projectile levels can be deduced. Combination with AM gives the fractions in the primary-ion beam.

OAM assumes conservation of the primary ion electron configuration during electron capture from a suitable atomic target, in particular alkali atoms. If such 'core conservation' holds, radiation observed from the final excited projectile directly shows which initial levels have been involved in the capture processes. The observed transition has to be characteristic for the initial ion-beam metastable component of interest. Matsumoto *et al.* [58] utilized this technique for determining the cross sections of ground-state $Ar^{2+}(3p^4\ ^3P)$, σ_{21}, and of metastable $Ar^{2+}(3p^4\ ^1D)$, σ^*_{21}, respectively, for one-electron capture from Na. Since these two cross sections are very similar, they could not be resolved by AM alone. With the assumption of core conservation in the one-electron capture process $Ar^+(3p^4[^3P]nl)$, i.e. $Ar^+(nl)$, ions come only from ground-state $Ar^{2+}(3p^4\ ^3P)$, $Ar^+(3p^4[^1D]nl)$, i.e. $Ar^+(nl')$, ions are only produced from metastable $Ar^{2+}(3p^4\ ^1D)$. Both final states $Ar^+(nl)$ and $Ar^+(nl')$ are excited and consequently emit characteristic light with intensity $S(x)$ and $S'(x)$, respectively, at position x along the beam axis:

$$S(x) \propto (1-f)\, I_0\, A_{nl}\, n_{Na}\, e^{-\sigma_{21} n_{Na}\, x}\,, \tag{2.6}$$

$$S'(x) \propto f\, I_0\, A_{nl'}\, n_{Na}\, e^{-\sigma^*_{21} n_{Na}\, x}\,. \tag{2.7}$$

f denotes the $Ar^{2+}(3p^4\ ^1D)$ fraction and I_0 the initial intensity of the primary-ion beam. n_{Na} is the Na target density, A_{nl} and $A_{nl'}$ the spontaneous emission coefficient of $Ar^+(nl)$

and Ar^+(nl'), respectively, σ_{21} and σ^*_{21} stand for the one-electron capture cross sections of $Ar^{2+}(3p^4\ ^3P)$ and $Ar^{2+}(3p^4\ ^1D)$, respectively. Therefore, σ_{21} and σ^*_{21} can be determined independently from the slopes of $\ln(S(x))$ and $\ln(S'(x))$ against $n_{Na}\,x$.

The Ar^{2+} ion beam attenuates as follows

$$I(L)/I_0 = (1-f)\,e^{-\sigma_{21} n_{Na}\,L} + f\,e^{-\sigma^*_{21} n_{Na}\,L}, \tag{2.8}$$

where $I(L)$ stands for the final Ar^{2+} intensity and L for the collision length. If the cross sections σ_{21} and σ^*_{21} are known from OAM measurements, the fraction of the metastable Ar^{2+} beam can be determined.

Brazuk *et al.* [61] extended the OAM to photon emission in the VUV spectral region in order to investigate electron capture in Ne^{2+}-Xe collisions and subsequently introduced a similar method utilizing **e**xcitation due to **c**ore **c**onserving electron **c**apture from alkali atoms ('X3C' method) which relies on relative measurements only [62]. The metastable fractions are derived from photon-signal ratios, which are determined for a sufficient number of beams with substantially different metastable ion-beam compositions. The X3C method has been successfully applied to beams of multiply charged ions (C^{2+}, N^{2+}, N^{3+}, and O^{4+}) from an ECR ion source as well as singly charged ions (C^+, N^+, and O^+ [63]).

Grazing incidence method

This rather new technique for analyzing fast metastable atomic beams makes use of effects of the image charge on projectile trajectories in scattering of fast beams on surfaces under grazing angles of incidence. Hecht *et al.* [60] analysed fast He beams on Al (111) surfaces. Metastable He atoms approaching the surface are ionized at about 14 a.u. distance to the surface. Consequently they are deflected and gain energy due to the image-charge force. When the distance to the surface has decreased to about 2 a.u., these He ions undergo Auger neutralization and are reflected from the surface as ground-state He atoms, but with a larger angle of reflection than the initial angle of incidence. Since ground-state He atoms are not ionized when approaching the surface, they are not affected by image forces and their angle of reflection equals the angle of incidence. Hence, ground-state- and metastable atoms are spatially separated during the scattering process. Detection of the beam densities of the separated beam components behind the surface yields the metastable fraction. The difficulties of this technique lie in the preparation of target and beam, i.e. the target surfaces have to be perfectly flat and the beam has to be well collimated.

2.1.2.2 Determination of the He Metastable Beam Fraction at IAP

The technique for measuring the metastable fraction of fast He-beams utilized during this work is similar to the optical attenuation method, but in contrast to the experiments by groups like Matsumoto *et al.* [58] and Brazuk *et al.* [61, 62], we base our measurements on excitation rather than electron capture.

In collisions between fast He beams and a target gas, excited projectile- and target atoms are produced. The intensity of the spontaneous emission from these excited states is proportional to their population density. Cross sections are particularly large for quasiresonant reactions. In a quasiresonant reaction the energy difference for the transition of the target atom matches closely the energy difference for the transition of the projectile. This is the case for excitation-transfer collisions between metastable He atoms and Ne, as utilized in the He-Ne laser. Figure 2.1 gives the energy-level diagrams of HeI- and NeI levels involved in excitation-transfer collisions between metastable He and ground-state Ne. For easier notation the levels Ne($1s^2\,2s^2\,2p^5$ nl) and Ne($1s^2\,2s^2\,2p^5$ nl') are summarized as Ne(nl,nl'). In quasiresonant excitation-transfer collisions between He(2^1S) and ground-state Ne the He atom is de-excited into the ground state. Its energy is transferred to the Ne atom, which is excited to Ne(5s,5s') and consequently decays to Ne(3p,3p'). In the case of quasiresonant excitation-transfer collisions between He(2^3S) and ground-state Ne the latter is excited into Ne(4s,4s'), which is followed by spontaneous emission to Ne(3p,3p') and consequently to Ne(3s,3s'). Finally, Ne(3s,3s') decays into Ne ground state.

A multitude of lines in a large wavelength range are emitted during these spontaneous emission processes due to the multiplicity of the Ne levels involved. The transition Ne(5s,5s') $\rightarrow$ Ne(3p,3p'), which is a measure for the initial He(2^1S) population, emits light at wavelengths between 543 nm and 773 nm. One of these emission lines, i.e. the 632.8 nm emission, is well known from He-Ne lasers. Emission lines of Ne(3p,3p') $\rightarrow$ Ne(3s,3s'), which are a measure for the total metastable He population (2^1S and 2^3S), occur between 540 nm and 808 nm. Hence, the two wavelength regions of Ne(5s,5s') $\rightarrow$ Ne(3p,3p') and Ne(3p,3p') $\rightarrow$ Ne(3s,3s') overlap. Table 2.4 shows emission lines of both transitions in the wavelength region between 625 nm and 641 nm.

From the measurements of Huber [65] using the same experimental setup we conclude that the emitted spectrum in the vicinity of 633 nm is dominated by the Ne(3p,3p') $\rightarrow$ Ne(3s,3s') transition (figure 2.2), as only the lines displayed in the right column of table 2.4 (e.g. 630.5 nm and 633.4 nm) are visible. The contribution from excitation transfer out

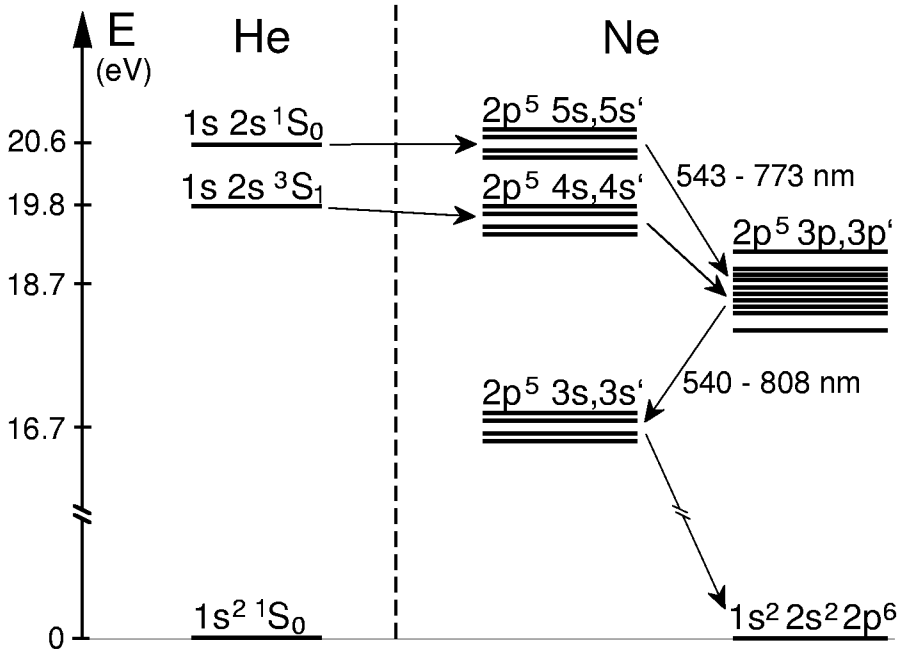

Figure 2.1: Energy levels involved in excitation-transfer collisions between metastable He atoms and ground-state Ne atoms and subsequent spontaneous emission of Ne.

Ne(5s,5s') → Ne(3p,3p')	Ne(3p,3p') → Ne(3s,3s')
629.4 nm	626.6 nm
631.4 nm	630.5 nm
632.8 nm	633.4 nm
633.1 nm	638.3 nm
635.2 nm	640.2 nm
636.5 nm	
640.1 nm	

Table 2.4: Wavelengths of transitions occurring during Ne(5s,5s') → Ne(3p,3p') and Ne(3p,3p') → Ne(3s,3s') spontaneous emission in the region between 625 nm and 641 nm [64].

of the 2^1S state, which yields lines displayed in the left column of table 2.4, were below our detection limit. Obviously the 2^1S state had already been efficiently quenched by residual gas atom collisions as mentioned in chapter 2.1.1. Consequently, the intensity of light observed with a 633 nm interference filter (see chapter 2.2.4) is a measure for the He(2^3S) population density.

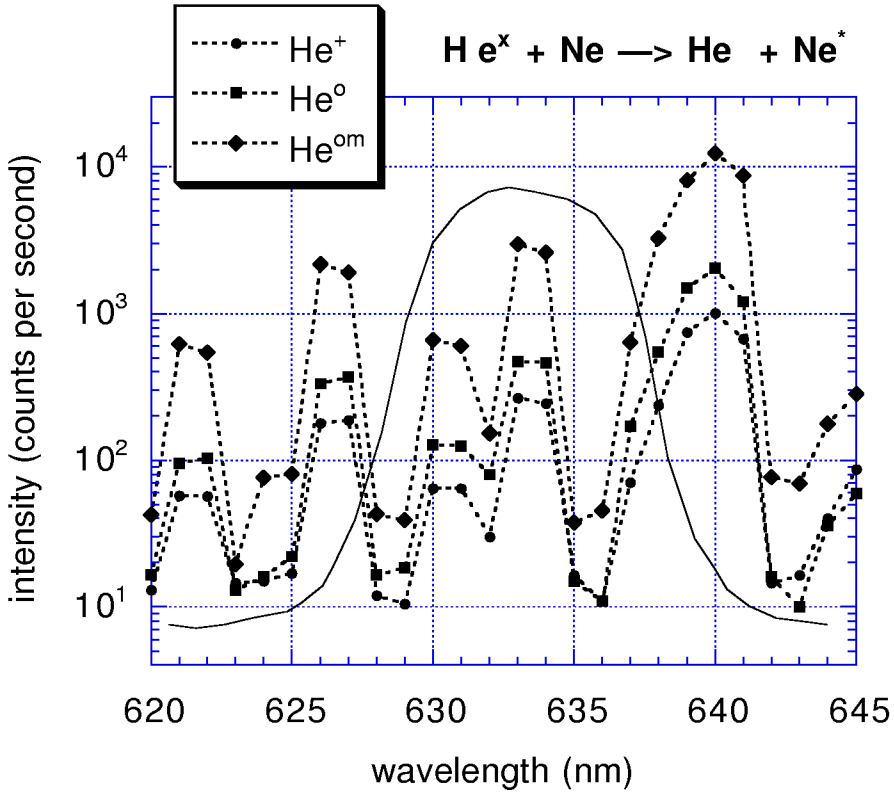

Figure 2.2: Emission spectrum of 10 keV He beams of different composition in Ne registered with a Czerny Turner spectrometer [65]. He^+ denotes an ion beam, He^o and He^{om} indicate He beams neutralized in He gas or Na vapour, respectively. Additionally, the transmission of the 633 nm interference filter used for the measurements presented in chapter 2.3 is shown (solid line).

Another process leading to a rather strong emission, characteristic for the initial $He(2^3S)$ population, is the excitation process $He(2^3S) \rightarrow He(3^3P)$. $He(3^3P)$ decays back to $He(2^3S)$ emitting at 389 nm. As the cross section for spin-changing collisions are negligibly small compared to spin-conserving collisions, the line intensity at 389 nm can be assumed to originate from $He(2^3S)$ only. Hence, the emission intensity observed at this wavelength can also be used as a measure for the initial $He(2^3S)$ fraction.

Several possibilities for determination of f have been suggested and discussed by Huber [65], e.g.:

- singlet/triplet He line-intensity ratios, e.g. 389 nm/502 nm,
- Ne line-intensity ratios,
- He/Ne line ratios,
- changes in intensity due to variation of beam composition.

As the 502 nm ($3^1P \rightarrow 2^1S$) emission is too weak, the first suggestion failed. Some other singlet and triplet emission lines exhibit sufficient intensity, e.g. 588 nm ($3^3D \rightarrow 2^3P$) and 668 nm ($3^1D \rightarrow 2^1P$). Prerequisite for determination of f is the knowledge of the corresponding excitation cross sections for collisions between He (ground state and 2^3S) and ground state Ne. Unfortunately, the relevant cross section databases (e.g. [54]) are not sufficiently complete.

Determination of f using Ne line-intensity ratios is problematic due to the multiplicity of the levels. To use only one line each for characterization of singlet or triplet metastables is not suitable as the relevant cross sections are not sufficiently well known.

Another idea was the calibration of the optical system at one characteristic wavelength (e.g. 633 nm or 389 nm) with beams exhibiting metastable fractions known from literature [49, 51, 52]. The beam composition can be adjusted by variation of the neutralization-target thickness, i.e. the product of target density and interaction length between beam and target (Na or He, see chapter 2.1.1).

In the present work, another method for determining f is introduced utilizing the variation of the beam composition with attenuation-target thickness. A collisional model has been developed for calculating the population-density progression of levels of interest during attenuation of the He beam in Ne gas. By adjusting the variable parameter f until the calculated Ne(3p,3p') $\rightarrow$ Ne(3s,3s') emission matches the measured Ne emission in the range selected by the 633 nm interference filter, the metastable fraction f of the incident beam can be deduced. A detailed description of this model is given in chapter 2.3.

2.2 Mixed He Beam Setup

The schematic view of the He-beam setup at IAP termed 'HELMA' (a composition of **hel**ium and **m**etastable **a**toms) is given in figure 2.3. A He ion beam is produced with a 2.45 GHz-ECRIS (**e**lectron **c**yclotron **r**esonance **i**on **s**ource [44, 45, 46]). By setting the ion source to high potential, He ions are extracted from the ion source and accelerated to several kV by an electrostatic accel-/decel system, and pass an electrostatic lens and a sector magnet which deflects the ions by 50° degree. The deflected monoenergetic ions pass the neutralization chamber [66, 47] either filled with Na vapour or He gas, and are removed from the beam by electrostatic deflection plates. The neutral particles enter an attenuation chamber [65] which is filled with neon gas, and are finally registered in a Faraday cup. Optical emission from

collisions between the neutral He- and the Ne-gas atoms is analysed by means of interference filters and a photomultiplier. The single parts of the setup are described in the following chapters.

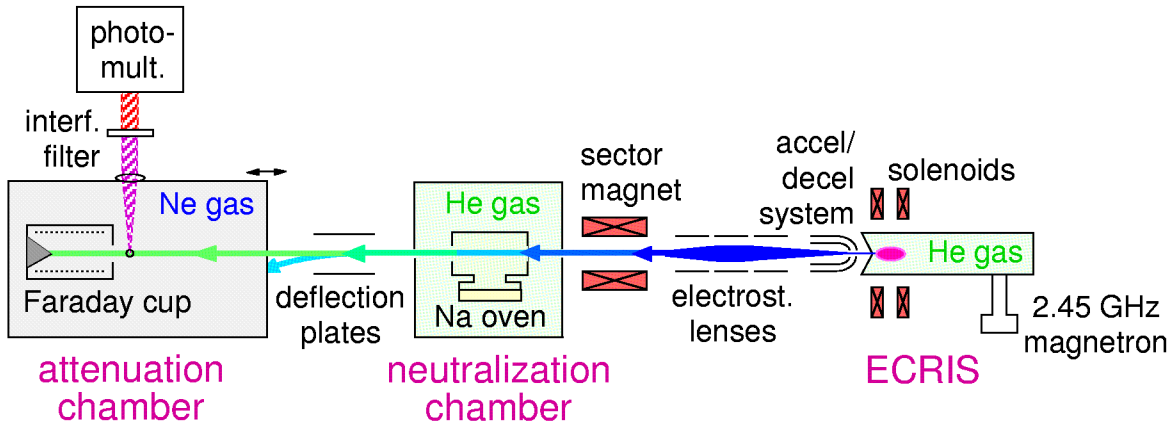

Figure 2.3: Schematic illustration of the He-beam setup HELMA.

2.2.1 2.45 GHz ECRIS

An ECRIS ion source consists of a confining magnetic field structure which also contains the resonance layer for electron-cyclotron radiation launched into the source. Electrons near the resonance region absorb the emitted radiation and are accelerated. The ions are produced in collisions of these accelerated electrons with the gas filled into the source. A detailed description of the 2.45 GHz-ECRIS at IAP can be found in [44, 46].

The plasma is trapped by the magnetic field of two solenoids positioned coaxially to the plasma tube (figure 2.3, [44, 45]). The solenoids produce a so-called magnetic mirror field $B(\vec{r})$, see figure 2.4.

Due to the invariance of the magnetic momentum μ,

$$\mu = \frac{m\, v_{\perp}^2(\vec{r})}{2\, B(\vec{r})}, \tag{2.9}$$

the charged particles with mass m are trapped in the magnetic mirror configuration depending on their velocity $v_{\perp}(\vec{r})$ perpendicular to the magnetic field $B(\vec{r})$. Increasing $B(\vec{r})$ leads to an increase in $v_{\perp}(\vec{r})$. As a result the velocity parallel to $B(\vec{r})$, $v_{\parallel}(\vec{r})$, decreases due to

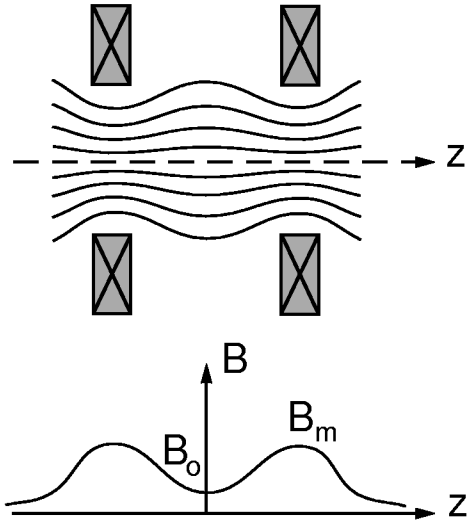

Figure 2.4: 'Minimum B' configuration generated by two solenoids positioned radially around the z-axis. Above: magnetic field lines, below: magnetic field at z-axis.

conservation of energy until becoming zero. At that position ($\vec{r}_r$), the particle velocity has only a perpendicular component, $v(\vec{r}_r) = v_\perp(\vec{r}_r)$, i.e. the particle is reflected at $\vec{r}_r$ and thus trapped in the magnetic field. Particles with $v_\parallel(z = 0) \equiv v_{\parallel o}$ above the critical velocity

$$v_{\parallel c} = \sqrt{\frac{2\,\mu}{m}(B_m - B_o)} \tag{2.10}$$

are able to escape the mirror field. B_o denotes the magnetic field at $z = 0$ and B_m the maximum magnetic field on the z-axis (see figure 2.4). In velocity space the region of the lost particles is cone shaped (so-called loss cone):

$$\left(\frac{v_{\perp o}}{v_o}\right)_c^2 = \frac{v_{\perp o}^2}{v_{\perp o}^2 + v_{\parallel c}^2} = \frac{B_o}{B_m} = sin^2\Theta_m. \tag{2.11}$$

The angle Θ_m determines the loss cone, which is equal for electrons and ions. Particle loss is determined by scattering into the loss cone predominantly due to Coulomb collisions. Electrons having a higher loss rate than ions due to their much higher collision frequency, cause a positive electrostatic potential, the so-called ambipolar potential Φ_a, which compensates for the difference in loss rates of electrons and ions.

As the magnetic field is not homogenous, the gyration frequency ω_{ce} of the electrons depends on its location in the plasma tube:

$$\omega_{ce}(r,\theta) = \frac{e\,B(r,\theta)}{m_e}. \tag{2.12}$$

r and θ denote radius and angle in cylindric coordinates. In the regions where ω_{ce} equals the microwave frequency the electrons will be accelerated. This results in a highly efficient ionization of the gas particles in that region. At 2.45 GHz this resonance occurs at a magnetic field of 87.5 mT which corresponds to a solenoid current of about 250 A in this geometry. Since the ion-gyration frequency is much lower than the electron gyration frequency ω_{ce} due to their large mass difference ($m_{He} \approx 8000\ m_e$), only the electrons are heated directly by the microwave.

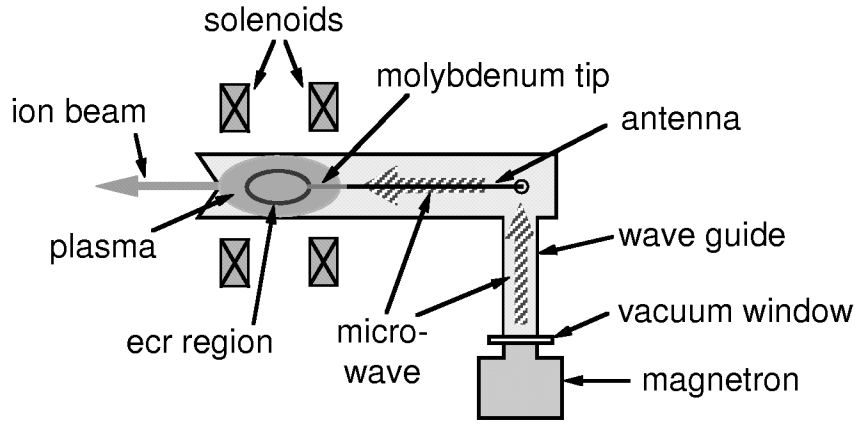

Figure 2.5: Schematic diagram of the 2.45 GHz ECRIS at IAP.

The heating microwave is generated in a water-cooled magnetron with an output power in the range of 200 W to 1.2 kW. It can be operated in continuous or pulsed mode. During the experiments conducted in this thesis the magnetron was used in continuous mode at about 300 W only. The microwave is directed via a rectangular wave guide and a 90° coupling into the cylindrical plasma tube to a coaxial molybdenum antenna [44, 45], see figure 2.5. The vacuum window in the rectangular wave guide consists of a 5 mm thick teflon plate which also serves as high voltage insulator. The antenna ends close to the ECR region. The extracted ions leave the ion source through the extraction aperture, in this case a Pierce-shaped electrode with an aperture of 3 mm diameter. The extracted current is of the order of several hundred μA.

The conductivity L_c (unit: m^3/s) for a hole with area F (unit: m^2) is given by [68]

$$L_c = 0.25\,\bar{v}\,F, \tag{2.13}$$

where $\bar{v}$ (unit: m/s) denotes the average particle velocity which for He at room temperature is $1.25{\cdot}10^3$ m/s. The conductivity of the plasma electrode is with $2.2{\cdot}10^{-3}$ m^3/s by a factor of 136 smaller than the pumping speed of the turbo pump (0.3 m^3/s) yielding a similar pressure ratio between plasma tube and extraction vessel. With a pressure in the plasma tube of about 10^{-3} mbar during operation, the pressure in the extraction vessel therefore amounts to about 10^{-5} mbar. This corresponds to a He gas density of about 10^{17} m^{-3}.

2.2.2 Beam Transport

The ion source is operated at a potential of up to +12.5 kV with respect to ground, the decel electrode is set to ground potential and the accel electrode to typically -2 kV. The ion optics is dominated by space charge and the focussing effect of electrostatic lenses. The beam trajectories can be further influenced by an electrostatic lens consisting of three cylindrical electrodes, see figure 2.3. The first and third electrodes are grounded and the second one is set to several kV. This leads to an electric field with high gradients in the gaps between the three electrodes, where the beam particles are accelerated or decelerated. As with the accel/decel system, an appropriate combination of acceleration and deceleration results in focussing of the ion beam [69].

In addition, a movable Faraday cup has been arranged in the vacuum region where the accel-/decel system and the first electrostatic lens are located. This Faraday cup is only moved into the beam path for coarse positioning of the beam, but not during routine operation of the system. Subsequently, the ion beam passes a second electrostatic lens system [70] with an inner diameter of 45 mm.

Ion beams produced from He gas in the 2.45 GHz ECRIS of IAP consist not only of He^+ but also contain unwanted beam components (He^{2+}, H^+ and H_2^+), as can be seen in figure 2.6. These components are eliminated by the 50° sector magnet. In the magnetic field of a sector magnet the beam particles are selected due to their mass/charge ratio. As no other beam particles with a mass/charge value similar to that of He^+ are expected in the beam, the He^+ beam can be considered as pure after passing the sector magnet.

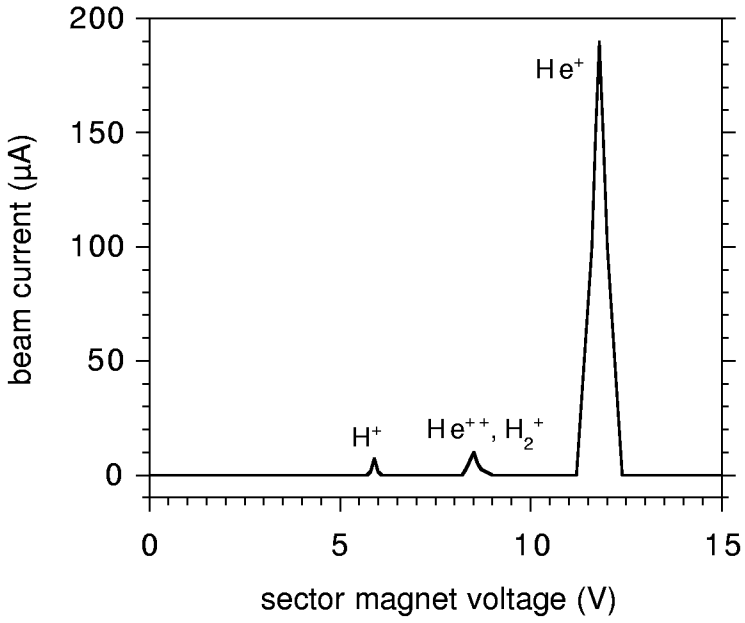

Figure 2.6: Ion beam spectrum taken after the sector magnet for a 12.5 keV He beam. Magnet settings are indicated by the voltage of the power supply.

2.2.3 Neutralization Chamber

The He-ion beam has been neutralized in either He gas or Na vapour. If He gas is used for charge-exchange, the resulting He-beam atoms are predominantly in ground state. Neutralization in Na leads to a He-atom beam with a considerable He(2^3S) fraction, see chapter 2.1.1.

The Na-vapour cell displayed in figure 2.7 has been made available to IAP by IPP Garching [71] and has been adapted to the HELMA setup in several ways [66, 47]. It consists of a cylindrical tube with 120 mm length and an inner diameter of 24 mm. In its center there is an opening to the Na reservoir mounted beneath. This opening can be closed by a plug mechanism from outside the vessel via a feedthrough, see figure 2.7. If the Na reservoir is closed, the ion beam can still pass the then empty tube of the Na-vapour cell. This is important for neutralization in He gas only.

In order to heat the neutralization tube and the Na reservoir, a thermocoax wire with 1 mm outer diameter is wrapped around them. It consists of an inner conductor with a resistivity of 12.5 Ω/m and an outer stainless steel tube isolated by ceramic powder. The temperature can be measured by four thermocouples, three at the tube and one at the reservoir. The vapour

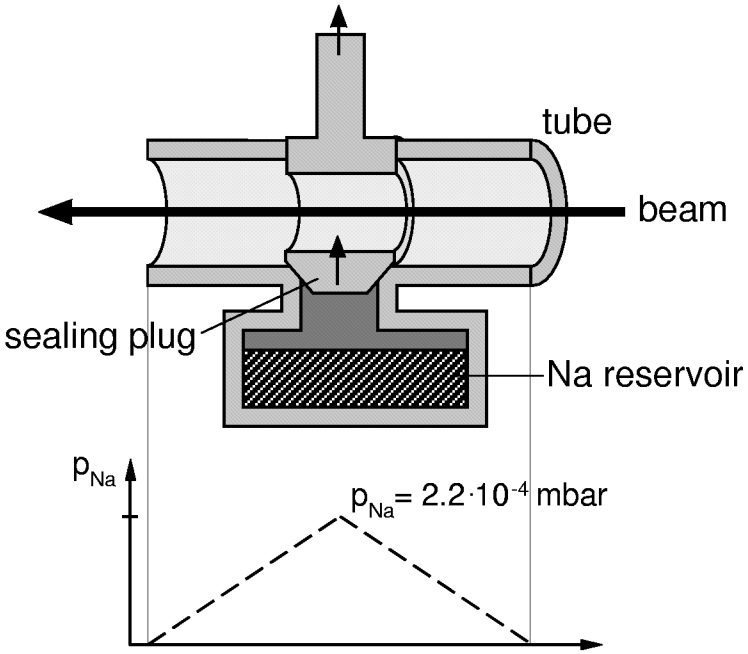

Figure 2.7: Schematic diagram of the Na-vapour cell at HELMA. Also shown is the Na-pressure distribution inside the tube for estimation of single collision condition, see text.

cell is heated to 200°C which corresponds to a Na-vapour pressure of $2.2{\cdot}10^{-4}$ mbar [50], i.e. a density of $3.4 \cdot 10^{18}$ particles per m^3. At this temperature, the Na in the oven is in liquid state (melting point 98°C [50]). The neutralization cell is located in the neutralization chamber (figure 2.3) which is pumped by a turbomolecular pump with 0.26 m^3/s pumping speed for He. A residual He-gas pressure of $3{\cdot}10^{-7}$ mbar could be achieved. This corresponds to a density of $7{\cdot}10^{15}$ He atoms per m^3, i.e. about 1/500 of the Na density. Hence, the probability for He-He collisions can be neglected compared to He-Na collisions.

Conflicting requirements exist for the target density in the neutralization cell. The interpretation of the measurement is most straightforward for single-collision conditions in which the target density is small enough to exclude multiple collisions between beam particles and target gas. However, the neutral fraction is initially proportional to the target density and the sensitivity of the detection system can set a lower limit for the target density. In the neutralizer of neutral beam systems (e.g. neutral beam diagnostics, heating beam systems) the target density is normally optimized towards the highest possible neutral beam flux. In our measurements the conditions were set as follows.

The probability P for collisions with cross section σ is given by

$$P = \sigma \int_0^L n_T(l)\, dl, \tag{2.14}$$

where n_T denotes the target density, l the line parameter along the beam path and L the interaction length. As a reasonable approach for single-collision conditions, P should be smaller than 10%.

The largest cross section for rearrangement of ground state- and metastable population fractions is ionization out of the metastable states. For collisions of 10 keV He(2^3S) in Na this cross section is smaller than $5{\cdot}10^{-20}$ m^2 [72]. Additionally, we assume a Na density distribution along the beam path as indicated in figure 2.7. This leads to a value for P of less than 0.01, which means that the chance for a He(2^3S) particle to become neutralized by a second collision with Na is smaller than 1%.

For using He gas as neutralizer, the neutralization chamber is filled with He gas through a precision valve on top of the charge-exchange vacuum vessel. The gas pressure can be measured by an ionization gauge. The neutralization chamber is closed off by two apertures with a diameter of 15 mm, and the distance between the two apertures is about 0.3 m. The cross section for charge exchange between 10 keV He ions and thermal He atoms is $6.1{\cdot}10^{-20}$ m^2 [73]. For the experiments presented in chapter 2.3, a He pressure of $3{\cdot}10^{-4}$ mbar was chosen, corresponding to a 15% chance for a He ion to be neutralized. A collision between two He atoms leads most likely to excitation into He(2^3S) ($\sigma \approx 10^{-20}$ m^2 [54]). Hence, the probability for an already neutralized He beam particle to get excited by a second collision with a He-gas atom is only 2%.

In the following vacuum vessel after the neutralization chamber an additional Faraday cup is located which can be moved into the beam if needed. The remaining ions are removed from the beam by a set of deflection plates.

2.2.4 Attenuation Chamber for Determination of the He Beam Composition

In this chamber, attenuation of the He beam in Ne gas is analysed by detecting the NeI emission at 633 nm and the HeI emission at 389 nm. Additionally, the beam particle flux is monitored by a specially designed neutral particle Faraday cup [67]. A detailed description of the attenuation chamber can be found in [65].

A schematic illustration of the attenuation chamber is given in figure 2.8. The chamber was filled with Ne gas via a needle valve. The beam passes the pre-chamber and enters the attenuation chamber through a 2 mm diameter aperture adjustable in beam direction. Its position determines the interaction length L of the beam in the gas target after which the beam reaches the observation position of the optical system and the Faraday cup. The attenuation chamber is connected with the pre-chamber also via a bypass which can be valved off. The pre-chamber is pumped with a 0.33 m^3/s turbomolecular pump. If the bypass valve is open, the residual gas pressure inside the attenuation chamber is less than 10^{-7} mbar. If the bypass valve is closed, the resulting pressure rises to about $5{\cdot}10^{-5}$ mbar while the He beam is on.

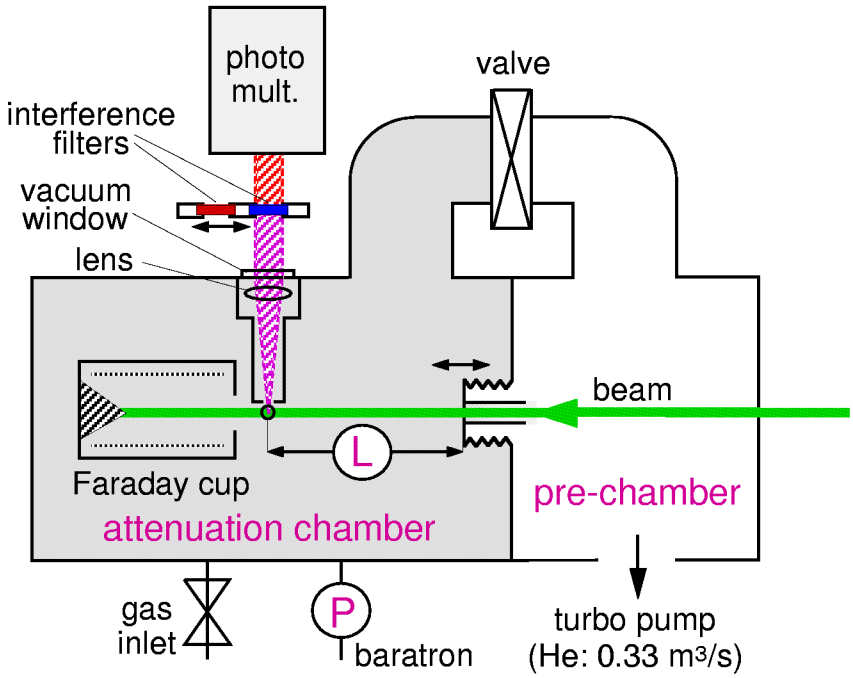

Figure 2.8: Schematic diagram of the attenuation chamber at HELMA.

Light emitted by the excited He- and Ne atoms reaches the photomultiplier via an optical system which consists of the following elements:

plano-convex lens	(Schott, 150 mm focal length, 90% transmission for 380 nm to 700 nm)
vacuum window	(borofloat quartz plate, Stölzle Oberglas, transmission $\geq$ 93% above 380 nm)
narrow-band interference filters	(Melles Griot 18F/I3900 10MK: 390 $\pm$ 4.5 nm, Melles Griot 03FIL026: 633 $\pm$ 5 nm, located in a moveable filter cassette)
photomultiplier	(EMI 9816B, 22% sensitivity at 380 nm, 8% sensitivity at 650 nm; Peltier-cooled)

The photomultiplier output is routed through a preamplifier, discriminator and to the LAB NB-card of the data acquisition system described in chapter 2.2.5. A hollow cylinder with a variable slit opening (0 to 3 mm) towards the beam was located between vacuum window and beam in order to narrow down the observed beam path region. In this way, a beam-path region of about 4 mm is imaged. The interference filters could easily be changed by shifting it within the filter cassette.

Assuming proportionality between the intensity S_{633} of the 633 nm emission and the He(2^3S) population, S_{633} is given by

$$S_{633} \propto n_{Ne}\, e^{-\sigma_m\, n_{Ne}\, L}, \tag{2.15}$$

where σ_m stands for the quenching cross section of He(2^3S) in Ne gas (density n_{Ne}), and L denotes the interaction length. In order to vary the target thickness $n_{Ne} \cdot L$, either the Ne pressure or the position of the beam entrance aperture (see figure 2.8) could be varied. The aperture can be moved with a stepper motor (dual stepper motor drive SMD2, Arun Microelectronics Ltd.) which is located outside the chamber. This motor is controlled by the LabVIEW program described in chapter 2.2.5. The gas pressure inside the chamber is measured with a baratron (MKS 627).

The beam was analysed with a specially designed Faraday cup [67] mounted behind the observation position. With this Faraday cup not only ion-beam currents but also the flux

of neutral beam particles can be measured. This 'neutral particle Faraday cup' (NPFC) is shown in figure 2.9.

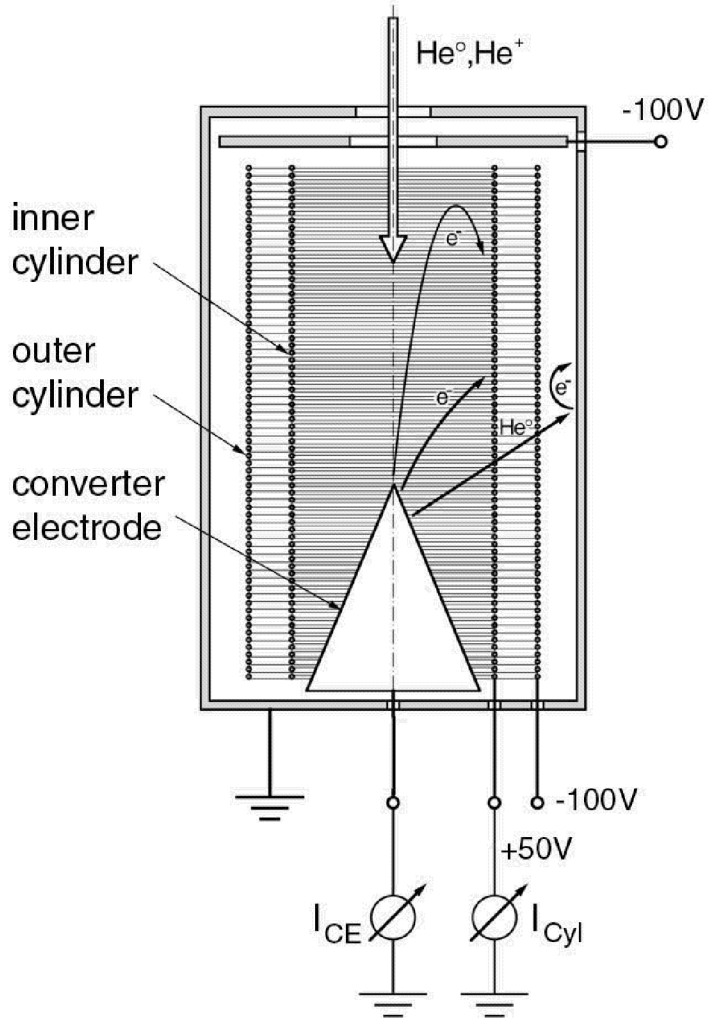

Figure 2.9: Schematic diagram of the NPFC at HELMA.

The Faraday cup consists of a grounded stainless steel housing. The beam enters the cup through a drilling (7 mm diameter) at the top, passes a negatively biased repeller electrode and hits the converter electrode made of stainless steel, which is surrounded by two cylinders made from wire mesh with 92% transparency. The inner cylinder acts as anode for secondary electrons released from the converter electrode by impact of beam particles. The outer cylinder is biased negatively and acts as reflector for the electrons passing through the anode mesh and also prevents secondary electrons from the housing wall to reach the anode.

In case of an incident beam consisting of both ions (current I_+) and atoms (equivalent current

I_o), the current at the converter electrode, I_{CE}, is given by

$$I_{CE} = I_+ + \gamma\,(I_+ + I_o)\,, \tag{2.16}$$

and the current at the inner cylinder, I_{Cyl}, by

$$I_{Cyl} = \gamma\,(I_+ + I_o)\,, \tag{2.17}$$

where γ denotes the electron-emission yield of the converter electrode, i.e. number of electrons emitted per incident beam particle. For a pure neutral beam, the neutral beam equivalent current I_o can be deduced by measuring the current I_{CE} at the converter electrode:

$$I_{CE} = \gamma\, I_o\,, \tag{2.18}$$

if γ is known. In principle, γ can be determined from a single measurement with a pure ion beam. But no ion beam with a negligible atom fraction could be produced due to neutralization of He^+ in the residual gas. Hence, γ was determined with two measurements, the first one with a beam consisting of ions and atoms and the second one with a pure atomic beam. At the beam energies used (several keV) potential electron emission is much weaker than kinetic electron emission [74]. Therefore, γ is assumed to be the same for He ions and atoms. From the measurements with on the one hand a beam consisting of ions and atoms ($I_{CE,1}$, $I_{Cyl,1}$) and on the other hand with a pure atomic beam ($I_{CE,2} = I_{Cyl,2}$), we get

$$\gamma = \frac{I_{Cyl,1} - I_{CE,2}}{I_{CE,1} - I_{Cyl,1}}\,. \tag{2.19}$$

During operation at room temperature, a time-dependent change of γ was observed [65]. This effect can be explained by adsorption of atoms and molecules (e.g. Na, H_20) on the converter surface. In order to reduce this adsorption to an acceptable value, the converter electrode is heated to 200°C. This is achieved by a thermocoax heater wrapped around a ceramic cylinder inside a hole drilled into the back side of the converter. Figure 2.10 shows experimentally deduced γ values for He beam energies between 3 keV and 12 keV.

The currents at cylinder, I_{Cyl}, and converter electrode, I_{CE}, are measured simultaneously with two picoamperemeters (Keithley 480), by which means the neutral particle flux I_o and the ion current I_+ can be deduced:

$$I_o = I_{Cyl}\,\frac{1+\gamma}{\gamma} - I_{CE}\,, \tag{2.20}$$

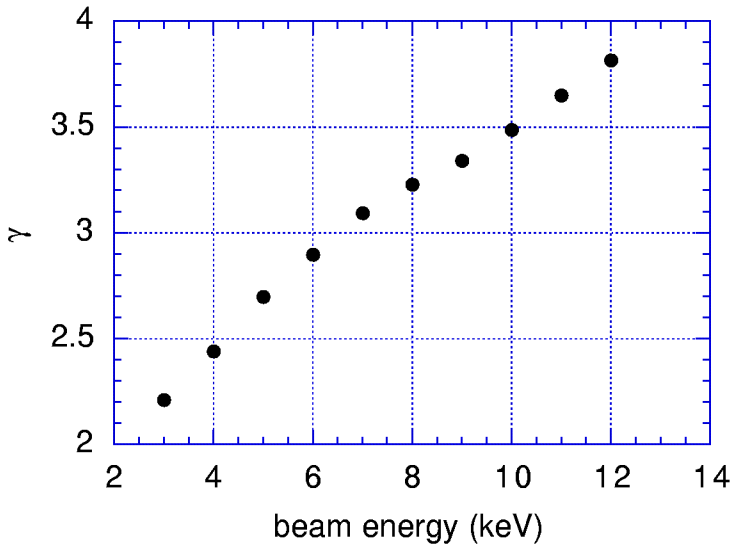

Figure 2.10: Experimentally deduced γ values for He atoms hitting the converter electrode of the NPFC [67].

$$I_+ = I_{CE} - I_{Cyl}\,. \tag{2.21}$$

The interaction length L has to be large compared with the distance $\tau{\cdot}v$, which the particle of velocity v travels between excitation and spontaneous emission of lifetime τ. If this is not the case, the measured beam emission S_M at the location viewed by the diagnostic system is not at the equilibrium level S_{LT}. To get the equilibrium level the measured quantity has to be corrected by the the following expression [75]:

$$S_{LT} = S_M\, F_{LT} = S_M \left(1 - \frac{\tau\, v}{\Delta L}\, e^{\frac{L}{\tau\, v}} \left(1 - e^{\frac{\Delta L}{\tau\, v}}\right)\right)\,. \tag{2.22}$$

ΔL stands for the extension of the observed beam path area. The lifetime of the considered HeI emission line at 389 nm amounts to $1.05{\cdot}10^{-7}$ s. Figure 2.11 shows F_{LT} values for this emission for three different beam energies.

2.2.5 Experiment Control and Data acquisition

The position of the aperture leading to the attenuation chamber and the data acquisition are computer controlled. This is done by an interactive LabVIEW program called 'current/counter/stepper' which controls a LAB NB-card (National Instruments Inc.).

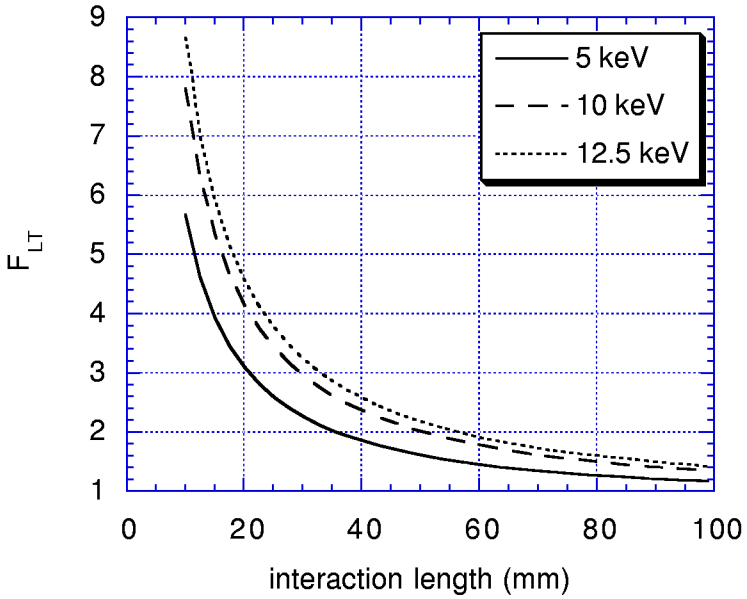

Figure 2.11: Lifetime correction factor F_{LT} of the 389 nm emission vs. interaction length of the beam in the target gas for three different beam energies.

The program reads photomultiplier counts and both cylinder- and converter-electrode current from the two picoamperemeters. For a better handling of beam-current fluctuations, the photomultiplier signal is normalized to the beam equivalent current. This is done by simultaneous integration of both the photomultiplier counting rate R_{PM} and the current I_{Cyl} with time t, until a charge

$$C_{Cyl} = \int_{t_1}^{t_2} \frac{I_{Cyl}}{\gamma}\, dt \tag{2.23}$$

has reached a pre-specified value. Hence, the value for the integrated photomultiplier signal

$$S_M = \int_{t_1}^{t_2} R_{PM}\, dt - R_B\,(t_2 - t_1) \tag{2.24}$$

is independent of beam-current variations. R_B denotes the photomultiplier background counting rate which is also determined with the program. The program can handle up to $6.5{\cdot}10^4$ counts per second and currents up to 2 mA.

Additionally, the program controls the movement of the aperture stepper motor. Parameters like direction of movement, distance for each step, and velocity of the movement can be chosen. It is also possible to move the aperture directly to a pre-defined position.

The output file contains the charge C_{Cyl}, last reading of cylinder- ($I_{Cyl}(t_2)$) and converter-electrode current ($I_{CE}(t_2)$), time elapsed during measurement ($t_2 - t_1$), and background-subtracted photomultiplier signal S_M.

An additional program can be used for calculating the electron yield γ by evaluation of I_{Cyl} and I_{CE} data for both pure neutral beams and beams containing neutrals and ions as described in chapter 2.2.4.

2.3 Results and Discussion

Neutral He beams in the energy range between 5 keV and 12.5 keV have been produced from He^+ ion beams passed through the neutralization chamber either filled with pure He gas ($3{\cdot}10^{-4}$ mbar) or with Na vapour from the vapour cell (200°C oven temperature). The beam neutralized in He gas consists predominantly of ground-state atoms (He^0), while the beam neutralized in Na contains a considerable fraction of metastable He atoms and will be called He^m- or mixed beam. He-ion beams in the energy range between 5 keV and 12.5 keV have been produced. The attenuation chamber was filled with Ne and the pressure was varied between $1{\cdot}10^{-4}$ and $1{\cdot}10^{-2}$ mbar. The location of the aperture of the attenuation chamber, which defines the interaction length, was chosen at 43 mm in front of the volume from which the beam emission was analyzed. The emission at 633 nm (NeI) and 389 nm (HeI) were measured. The photomultiplier signals were summed up until the charge C_{Cyl} in the neutral-particle Faraday cup reached 90 μC. The measured photomultiplier signals were lifetime- and background corrected as described in chapter 2.2.4. Examples from He^0- and He^m beams with three different beam energies are given in figures 2.12 and 2.13. As expected, the intensity of both emission lines is quite different for beams with low and high 2^3S fraction and could indeed be used to measure the metastable triplet fraction as proposed by [65]. Furthermore, the 633 nm emission yields about twice as much photomultiplier counts as the 389 nm emission.

Quantitative analysis of the 2^3S fraction has been done by comparing the experimental 633 nm intensity with that from a newly developed model, i.e. a simple 3-level model for calculating the He beam attenuation during collisions with Ne atoms and the resulting NeI emission at 633 nm. Figure 2.14 shows the transitions between He(1^1S), He(2^3S), and He^+ levels which are included in our simplified model. The corresponding collisions and cross sections are given in table 2.5.

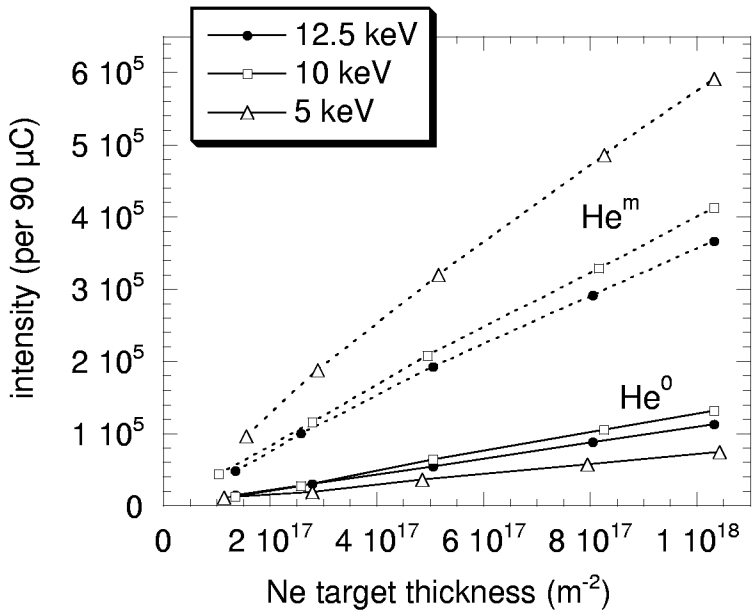

Figure 2.12: Photomultiplier signal (per 90 μC at the inner cylinder) versus Ne-gas thickness ($\hat{=}$ $1{\cdot}10^{-4}$ - $1{\cdot}10^{-3}$ mbar) using a HeI 389 nm filter for a He^+ beam neutralized in He gas (He^0) or Na vapour (He^m).

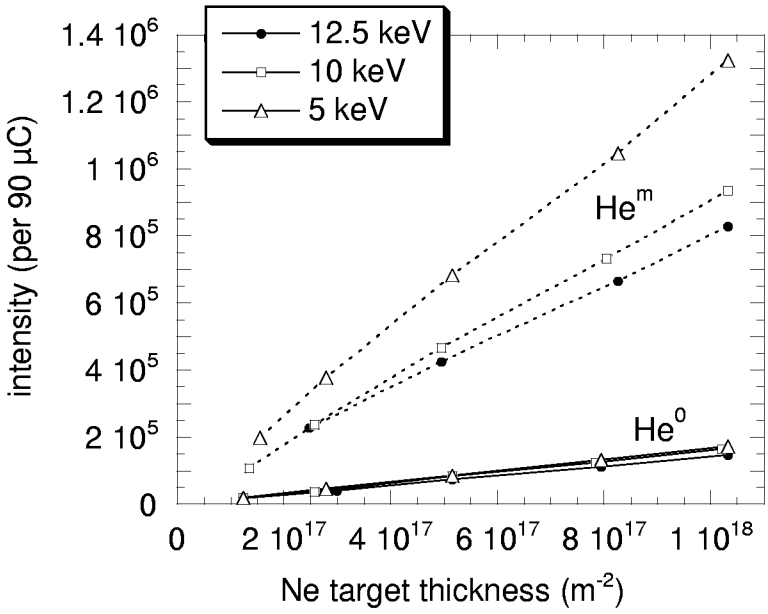

Figure 2.13: Photomultiplier signal (per 90 μC at the inner cylinder) versus Ne-gas thickness ($\hat{=}$ $1{\cdot}10^{-4}$ - $1{\cdot}10^{-3}$ mbar) using a NeI 633 nm filter for a He^+ beam neutralized in He gas (He^0) or Na vapour (He^m).

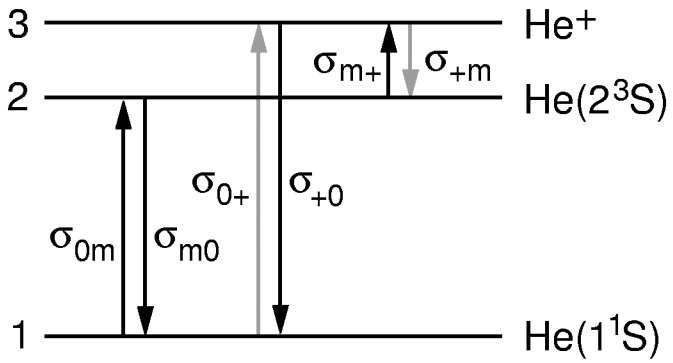

Figure 2.14: Levels and transitions included in the 3-level model for He-Ne collisions. Also displayed are the corresponding cross sections. The grey arrows mark the transitions which can be neglected due to their small cross section.

collisional process	cross section at 10 keV
$He(1^1S) + Ne \rightarrow He(2^3S) + Ne$	σ_{0m}
$He(2^3S) + Ne \rightarrow He(1^1S) + Ne(4s,4s')$	$\sigma_{m0} \approx 9{\cdot}10^{-20}$ m^2 [72, 76]
$He(2^3S) + Ne \rightarrow He^+ + Ne + e^-$	$\sigma_{m+} = 1.8{\cdot}10^{-21}$ m^2 [77]
$He^+ + Ne \rightarrow He(2^3S) + Ne^+$	$\sigma_{+m} \ll 10^{-20}$ m^2 [75, 73]
$He(1^1S) + Ne \rightarrow He^+ + Ne + e^-$	$\sigma_{0+} \ll 10^{-20}$ m^2 [72]
$He^+ + Ne \rightarrow He(1^1S) + Ne^+$	$\sigma_{+0} = 7.55{\cdot}10^{-20}$ m^2 [73, 78]

Table 2.5: Collisions included in the He-Ne model and cross sections at 10 keV as far as known from literature.

Some of the cross sections could either be found in literature in the wrong energy range only (σ_{m0}, σ_{+m}, and σ_{0+}), or could not be found at all (σ_{0m}). Only the values for σ_{m+} and σ_{+0} are given in the literature in the here considered energy range [77, 73, 78]. The cross section for the excitation transfer process, σ_{m0}, was found for lower (thermal He beams [76]) and higher ($\geq$ 50 keV [72]) beam energies and was estimated to be close to that of the thermal He beam, i.e. $9{\cdot}10^{-20}$ m^2. From extrapolation of the values for σ_{+m} [75, 73] and σ_{0+} [72] to the considered energy range, they have been assumed as negligibly small compared to the cross sections of the reverse processes. σ_{0m} was used as a free parameter in the modelling with the limitation of being small compared to the reverse collision cross section σ_{m0} since the latter is a resonant process. Hence, the balance equations for the three levels can be written as:

$$
\begin{aligned}
\frac{dn_{He(1^1S)}}{dx} &= n_{Ne}\left[-n_{He(1^1S)}(x)\,\sigma_{0m} + n_{He(2^3S)}(x)\,\sigma_{m0} + n_{He^+}(x)\,\sigma_{+0}\right] \\
\frac{dn_{He(2^3S)}}{dx} &= n_{Ne}\left[n_{He(1^1S)}(x)\,\sigma_{0m} - n_{He(2^3S)}(x)\,(\sigma_{m0} + \sigma_{m+})\right] \\
\frac{dn_{He^+}}{dx} &= n_{Ne}\left[n_{He(2^3S)}(x)\,\sigma_{m+} - n_{He^+}(x)\,\sigma_{+0}\right]
\end{aligned}
\tag{2.25}
$$

A mathematica code was developed in order to solve these balance equations and calculate the normalized intensity of the NeI 633 nm line given by

$$
\frac{S_{633}(x)}{n_{Ne}} \propto n_{He(2^3S)}(x)\,\sigma_{m0} + n_{He(1^1S)}\,\sigma_{0*}\,, \tag{2.26}
$$

where σ_{0*} denotes the cross section for the excitation reaction

$$
\mathrm{He}(1^1\mathrm{S}) + \mathrm{Ne} \rightarrow \mathrm{He}(1^1\mathrm{S}) + \mathrm{Ne}(4\mathrm{s},4\mathrm{s}'),
$$

which is assumed to be much smaller than σ_{m0}. This cross section could not be found in the literature either and, hence, it is used as free parameter in the modelling. The third free parameter is the $\mathrm{He}(2^3\mathrm{S})$ fraction

$$
f = \frac{n_{He(2^3S)}}{n_{beam}} = \frac{n_{He(2^3S)}}{n_{He(1^1S)} + n_{He(2^3S)}}, \tag{2.27}
$$

where n_{beam} stands for the total density of the beam atoms.

The calculations have been performed by attenuation of 10 keV He beams with two different He-beam compositions (He^0 and He^m) in Ne gas up to a pressure of $1{\cdot}10^{-2}$ mbar, where already multiple collisions occur which are included in the model. The measurement results given in figure 2.15 show a slightly increasing normalized intensity for the He^0 beam which consists mainly of ground-state atoms, and a rapidly decreasing one for the He^m beam with a high $\mathrm{He}(2^3\mathrm{S})$ fraction f. This can be qualitatively explained by an increase in the metastable fraction for the He^0 beam (more $\mathrm{He}(2^3\mathrm{S})$ produced than destroyed) whereas in the case of the He^m beam the destruction rate for $\mathrm{He}(2^3\mathrm{S})$ is larger than the production rate. As expected, the emitted normalized intensities of both beams have to converge to the same value for sufficiently thick targets. The calculation results exhibit the same attenuation behaviour as the measurements, which can be seen in figure 2.16.

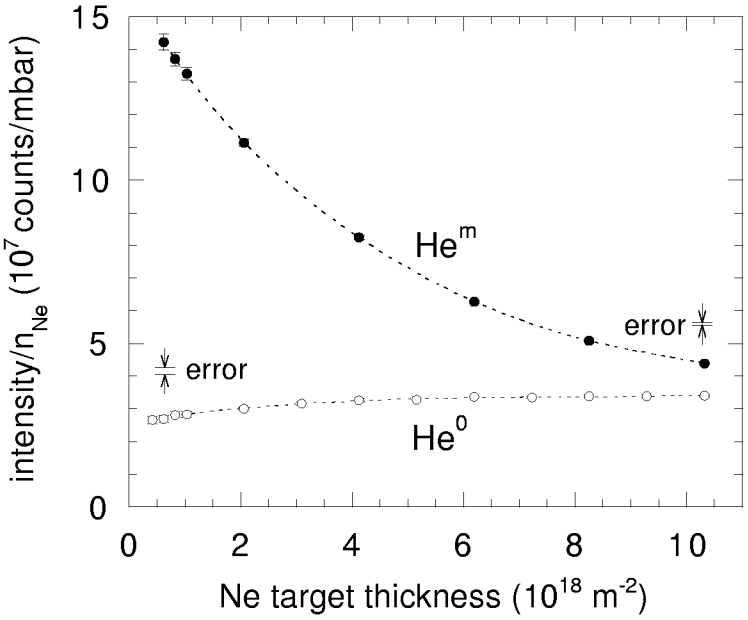

Figure 2.15: Normalized 633 nm emission of a 10 keV He beam neutralized either in Na vapour (He^m) or in He gas (He^0) vs. target thickness derived from measurement. The errors decrease with increasing target thickness as indicated in the figure. The dashed line is a polynomial fit.

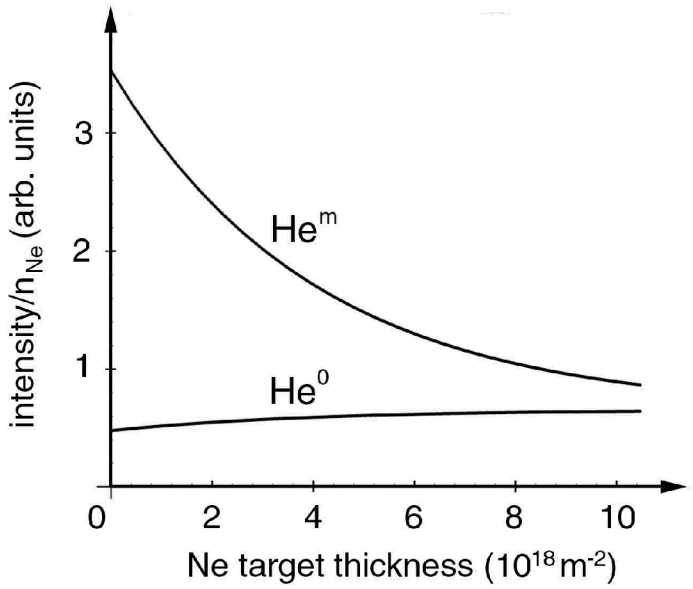

Figure 2.16: Progression of the normalized 633 nm emission calculated with the 3-level He-Ne model for a 10 keV He beam with either 80% (He^m) or 3% (He^0) metastable triplet fraction vs. target thickness.

The free parameters f, σ_{0m}, and σ_{0*} were optimized so that the shape of the normalized 633 nm intensity vs. target thickness for both He^m- and He^0 beam fitted the corresponding calculated curves. A reasonable match could be achieved for the following values of the cross sections:

$$\sigma_{0m} \approx \sigma_{0*} \approx 8{\cdot}10^{-21}\ \mathrm{m}^2.$$

The resulting values for the metastable triplet fractions are:

$$f(He^m) \approx 0.80, \text{ and}$$

$$f(He^0) \approx 0.03,$$

i.e. about 80% of the He^m-beam atoms and about 3% of the He^0-beam atoms are in metastable triplet state when entering the attenuation chamber. As mentioned above the exact value of f depends on the values of the cross sections used for the modelling. The considered values have been obtained with reasonable assumptions for the cross sections and have to be regarded as approximate.

From these measurements and calculations it can be concluded that with the He-beam setup HELMA we are able to produce He-atom beams with high metastable triplet fractions of up to about 80%. Furthermore, it is in principle possible to determine the triplet metastable fraction by comparing the measured and modelled beam attenuation. However, the cross-section database would have to be extended for a more precise evaluation. For the characterization of these mixed beams the emission at 633 nm is suitable for monitoring the metastable triplet fraction.